

---

# High Accuracy Pulmonary Vessel Segmentation for Contrast and Non-contrast CT Images and Its Clinical Evaluation

---

Ying Ming<sup>1</sup>, Shaoze Luo<sup>2</sup>, Longfei Zhao<sup>2</sup>, Qiqi Xu<sup>2</sup>, and Wei Song<sup>1,\*</sup>

**1 Department of Radiology, Peking Union Medical College Hospital, Chinese Academy of Medical Sciences and Peking Union Medical College, Beijing 100730, China**

**2 Research and Development Center, Canon Medical Systems (China), No.3, Xinyuan South Road, Chaoyang District, Beijing 100027, China**

## ABSTRACT

Accurate segmentation of pulmonary vessels plays a very critical role in diagnosing and assessing various lung diseases. In clinical practice, diagnosis is typically carried out using CTPA images. However, there is a lack of high-precision pulmonary vessel segmentation algorithms for CTPA, and pulmonary vessel segmentation for NCCT poses an even greater challenge. In this study, we propose a 3D image segmentation algorithm for automated pulmonary vessel segmentation from both contrast and non-contrast CT images. In the network, we designed a Vessel Lumen Structure Optimization Module (VLSOM), which extracts the centerline of vessels and adjusts the weights based on the positional information and adds a Cl-Dice-Loss to supervise the stability of the vessels structure. In addition, we designed a method for generating vessel GT from CTPA to NCCT for training models that support both CTPA and NCCT. In this work, we used 427 sets of high-precision annotated CT data from multiple vendors and countries. Finally, our experimental model achieved Cl-Recall, Cl-DICE and Recall values of 0.879, 0.909, 0.934 (CTPA) and 0.928, 0.936, 0.955 (NCCT) respectively. This shows that our model has achieved good performance in both accuracy and completeness of pulmonary vessel segmentation. In clinical visual evaluation, our model also had good segmentation performance on various disease types and can assist doctors in medical diagnosis, verifying the great potential of this method in clinical application.

## Introduction

Accurate and comprehensive segmentation of pulmonary vasculature is essential for diagnosing various pulmonary diseases, planning treatments, and monitoring disease progression<sup>[1,2,3]</sup>. Computed Tomography Pulmonary Angiography (CTPA) and Non-Contrast Computed Tomography (NCCT) are two widely used imaging modalities in clinical practice. While CTPA provides detailed vascular information due to the administration of contrast agents, NCCT lacks such enhancement but remains valuable for specific clinical scenarios, such as patients with contraindications to contrast media. Developing a unified framework that can effectively process both CTPA and NCCT data is therefore highly desirable<sup>[4,5]</sup>. Current research focuses more on CTPA data, which is easier to segment the pulmonary vessel, while there is less research on NCCT<sup>[6,7]</sup>. However, in many cases, NCCT is also worthy of model attention due to its easier access and lower radiation dose<sup>[8,9]</sup>. Moreover, existing works on pulmonary vessel segmentation often do not consider the integrity of the vascular lumen structure, focusing instead primarily on global statistical metrics such as DICE<sup>[10,11]</sup>. This tendency can easily lead to models being unable to effectively identify and segment distal small vessels, thereby impacting their practical performance.

In this study, we propose a deep learning-based three-dimensional pulmonary vessel segmentation model that leverages both CTPA and NCCT datasets. A key innovation of our approach lies in the design of a Vessel Lumen Structure Optimization Module (VLSOM). This module enhances the traditional 3D U-Net architecture by extracting vessel centerlines and applying weight-adjusted supervision during training. By incorporating these structural cues, the model achieves high segmentation accuracy while preserving the completeness of vascular structures. In terms of GT annotation, we have designed an annotation scheme that allows us to simultaneously obtain high-precision GT results for both CTPA and NCCT. This enables the trained segmentation model to support automatic segmentation of both types of data. In terms of evaluation, we added CI-DICE and CI-Recall to evaluate the results, emphasizing the quantitative analysis of the accuracy and integrity of the vascular lumen structure.

The resulting pulmonary vessel segmentation algorithm offers several advantages: high precision, comprehensive vascular representation, and compatibility with both CTPA and NCCT data. These features make it a promising tool for aiding clinical diagnosis and analysis. In the subsequent sections, we will elaborate on the methodology, experimental results, and potential applications of this novel AI-driven model in pulmonary imaging.

Furthermore, our model demonstrates strong performance in segmenting pulmonary vessels from CTPA data, enabling precise separation of arteries and veins. More importantly, through segmentation performance transfer from CTPA to NCCT, the model successfully extends its applicability to NCCT data. This capability not only addresses the limitations of existing methods that typically focus on a single modality but also broadens the clinical utility of the proposed algorithm.

## **1. Data**

### **a. Internal Data information**

In this study, a total of 427 cases were collected to develop and evaluate the proposed pulmonary vessel segmentation model. The dataset consisted of two main sources: 112 cases from the publicly available LIDC (Lung Image Database Consortium) dataset<sup>[12]</sup> and 315 cases from a private clinical dataset. To ensure comprehensive support for both CTPA (Computed Tomography Pulmonary Angiography) and NCCT (Non-Contrast Computed Tomography) data, the dataset included 213 CTPA cases and 214 NCCT cases. This balanced distribution across modalities facilitated the development of a versatile model capable of handling both contrast-enhanced and non-contrast imaging data.

The dataset was divided into two subsets for model development: 370 cases for training and 57 cases for testing. The training set contained 185 CTPA cases and 185 NCCT cases, while the testing set included 28 CTPA cases and 29 NCCT cases. This stratified partitioning strategy ensured that the model was trained and evaluated on data that reflected the diversity of clinical scenarios encountered in real-world applications.

The scanning equipment used for the mentioned experimental data includes devices from Canon, GE, Siemens, and Philips, involving diseases such as Pulmonary Nodules, Calcification, Emphysema, Pneumonia, Pleural Effusion, Pulmonary Mass, etc. The data sources encompass multiple hospitals from Asian countries as well as European countries. In all experimental data, the Z-direction resolution of CTPA ranges from 0.4 to 1.5 mm, the Z-direction resolution of NCCT ranges from 0.5 to 1.25 mm.

### **b. Internal Data Annotation**

Ground truth (GT) annotations were performed by two radiologists with more than ten years of working experience to ensure high-quality supervision during

model training. The annotation standard required labeling vessels as small as 1 mm in diameter, ensuring that even fine vascular structures were captured. This meticulous annotation process was critical for achieving high precision in vessel segmentation and preserving the completeness of the vascular network. In addition, the lung contours of each data were additionally annotated.

Annotating blood vessels in 3D CT images is a challenging task, which is difficult and labor-intensive for doctors to annotate directly. Therefore, we designed a data annotation scheme, and the complete ground truth (GT) generation process is shown in the figure below. Given that there are already preliminary algorithms supporting automatic segmentation of CTPA data, we first used semi-automatic segmentation method based on Hessian matrix<sup>[13]</sup> to generate an initial vascular tree (C0) on CTPA data, but it suffers from incomplete vascular branches and segmentation errors. We then used our self-developed annotation tool for doctors to carefully correct and supplement annotations (S0), ultimately obtaining a more complete and accurate annotation of the vascular branches in CTPA images (C1). To support the model's application to NCCT data, we trained a CTPA-based segmentation network using S1 and applied this network to NCCT data to obtain an initial vascular tree (N0). The above annotation process was repeated to finally achieve refined vessel annotations (N1) for NCCT data. The annotation process is shown in **Figure 1**, and the GT example of this dataset is shown in **Figure 2**.

In summary, the dataset used in this study was carefully curated to include a diverse range of cases from both public and private sources, with balanced representation of CTPA and NCCT data. The high-quality annotations and thoughtful data partitioning provided a strong foundation for developing a clinically relevant and versatile pulmonary vessel segmentation model. In the following sections, we will detail the methodology and experimental results.

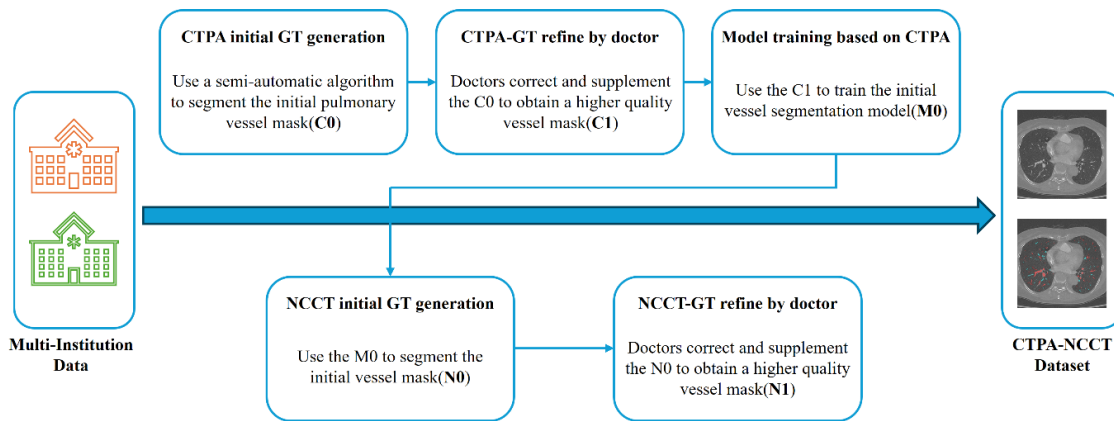


**Figure1 Iterative generation process of GT annotations of CTPA-NCCT**

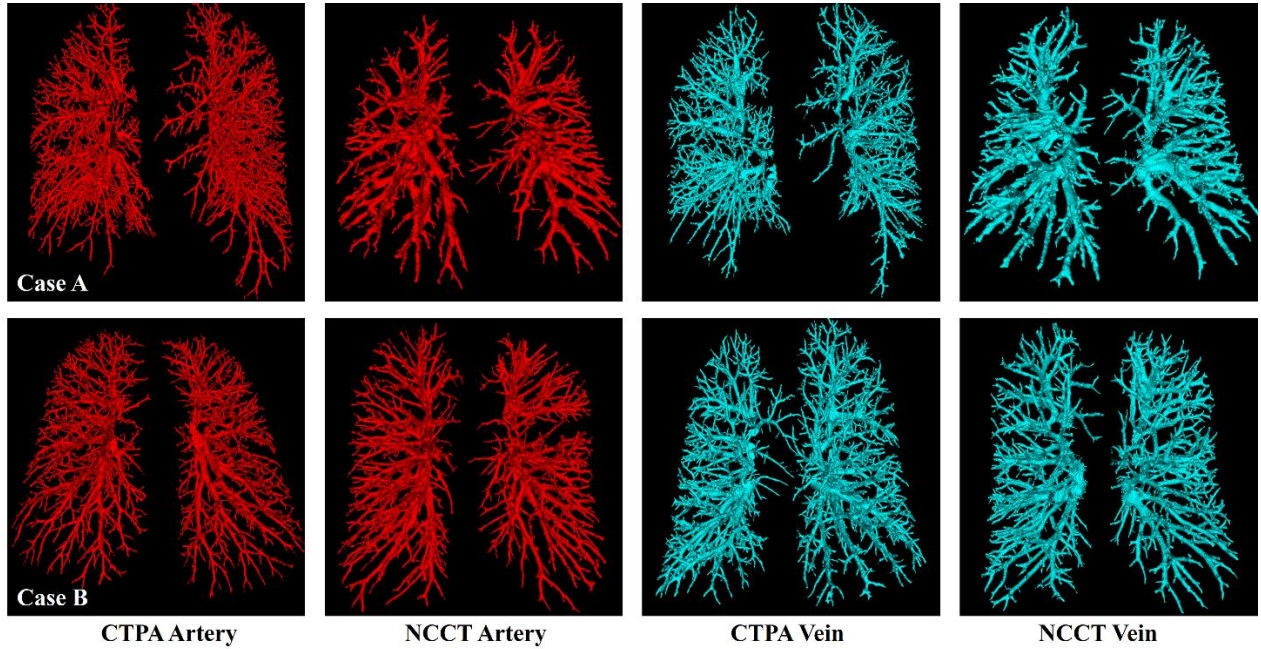


**Figure2** GT examples of experimental datasets

## 2. Method

The pulmonary artery and vein separation algorithm is designed to classify voxels into three categories: background, pulmonary arteries, and pulmonary veins. The method involves several key steps, including data preprocessing, model design, and post-processing part. Below, we detail each component of the pipeline. The overall process of this design method is shown in **Figure 3**, and the network structure (S2-1) of the model is shown in **Figure 4**.

### a. Data Preprocessing

The preprocessing pipeline plays a critical role in preparing the CT images for efficient and accurate analysis by the deep learning model. The specific preprocessing steps are outlined below: (1) Lung Region Cropping: To focus on the region of interest (ROI) and reduce unnecessary background information, the CT images are first cropped based on the bounding box of their lung masks; (2) Resampling: The cropped images are then resampled to a target isotropic resolution of  $0.726\text{mm} \times 0.726\text{mm} \times 0.8\text{mm}$ . This step ensures uniformity in voxel size across all datasets, addressing variations in the original imaging resolutions and facilitating consistent feature extraction by the model. (3) Intensity Normalization: To improve the robustness of the model to variations in image intensity, the intensity values of

the resampled images are clipped to the range between the 0.5th percentile and the 99.5th percentile of the image foreground intensity values.

## **b. Model Design**

The backbone of our model is based on the 3D U-Net architecture<sup>[14]</sup>, which has demonstrated strong performance in medical image segmentation tasks due to its encoder-decoder structure with skip connections. To improve the segmentation of vascular structures, we introduce the Vessel Lumen Structure Optimization Module (VLSOM). This module extracts the centerlines of the ground truth (GT) vessels and incorporates them as additional supervisory signals during training. The three main modules include: (1) Vessel Centerline Extraction Outline: The GT vascular masks are processed to extract their centerlines. These centerlines serve as a structural cue to guide the model in identifying and preserving the fine details of vessel lumen structures; (2) Weighted Supervision: Based on clinical experience and pre-experimental results, the VLSOM applies different weights to the vessel regions based on their proximity to the centerlines. This ensures that the model pays more attention to the centerline regions during training, thereby improving the precision of vessel segmentation; (3) Loss function design:

$$Loss = CE Loss + DICE Loss + 0.5 CL_{DICE} Loss$$

$$Weight CE Loss = (\omega_{class} = 3, \omega_{cl} = 15)$$

$$Weight DICE Loss = (\omega_{class} = 3, \omega_{cl} = 15, in lung mask)$$

$$Weight CL_{DICE} Loss = (\omega_{class} = 3, \omega_{cl} = 15, in lung mask)$$

Here,  $\omega_{class}$  represents the training weight for the non-centerline regions of the vessels, while  $\omega_{cl}$  represents the training weight for the centerline regions of the vessels. The notation "in lung mask" indicates that this weighting logic is only effective within the lung region and no additional weighting is applied outside the lung area. The above DICE Loss<sup>[15]</sup> and CLDICE Loss<sup>[16]</sup> are both loss functions based on the vessel contour structure.

The network was configured with 32 base channels and 17 convolutional layers, using a patch size of [192,256,96] for efficient training. It was trained for 1000 epochs with an initial learning rate of 1e-2, which decayed by 3e-5 every 50 epochs. The Adam optimizer was used to adaptively adjust the learning rates during training, ensuring stable convergence and effective parameter optimization. We used the NVIDIA Tesla A800 80G for model training and testing.

## **c. Post-Processing**

After model inference on the cropped volume, we designed a post-processing algorithm to remove outliers and adjust disconnected vessel branches. The steps of the post-processing algorithm are as follows: (1) Connected Component Analysis: Calculate the connected components for both the artery and vein domains. (2) Remove Outliers: Eliminate any connected components that lie entirely outside the lung mask. (3) Select Largest Components: Identify and select the largest connected components for both arteries and veins. (4) Handle Disconnected Artery Components: If small disconnected artery components (size < threshold voxels) are connected to the largest vein component, reclassify these small artery components as veins and update the largest vein component. (5) Handle Disconnected Vein Components: If small disconnected vein components (size < threshold voxels) are connected to the largest artery component, reclassify these small vein components as arteries and update the largest artery component. (6) Iterative Refinement: Repeat steps 4 and 5 iteratively until no additional small components can be connected to either the artery or vein. In this experiment, the default threshold is set to 800.

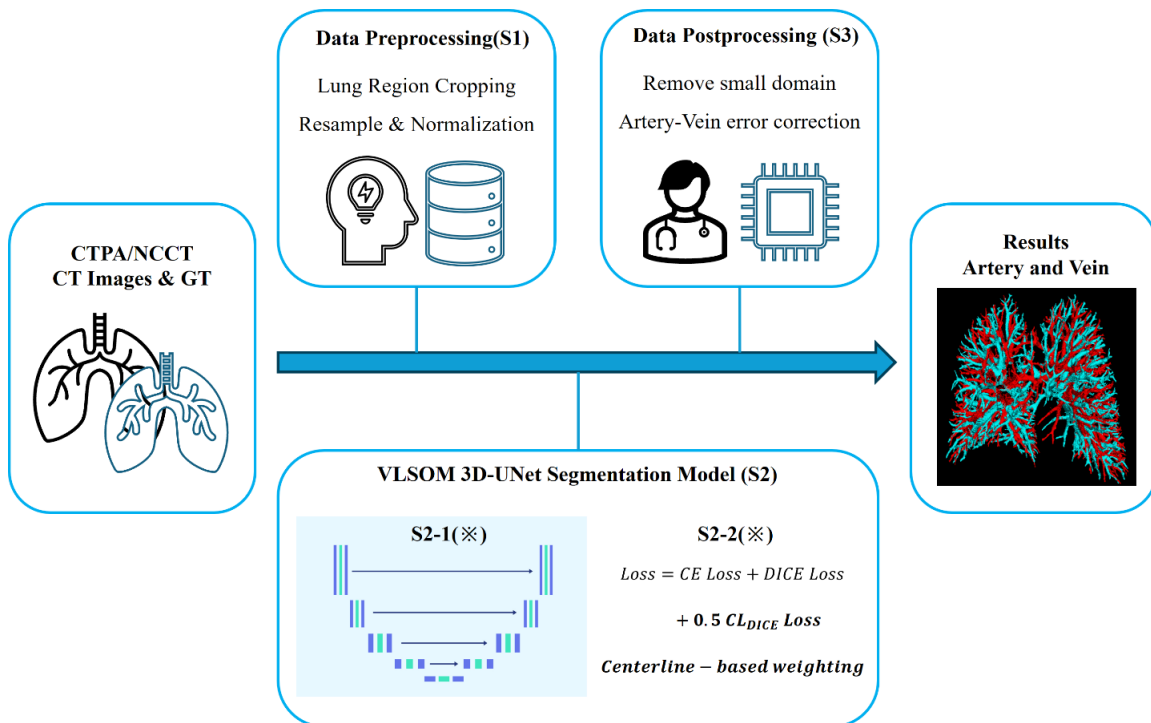


**Figure3** The main structure of the pulmonary vessel segmentation model

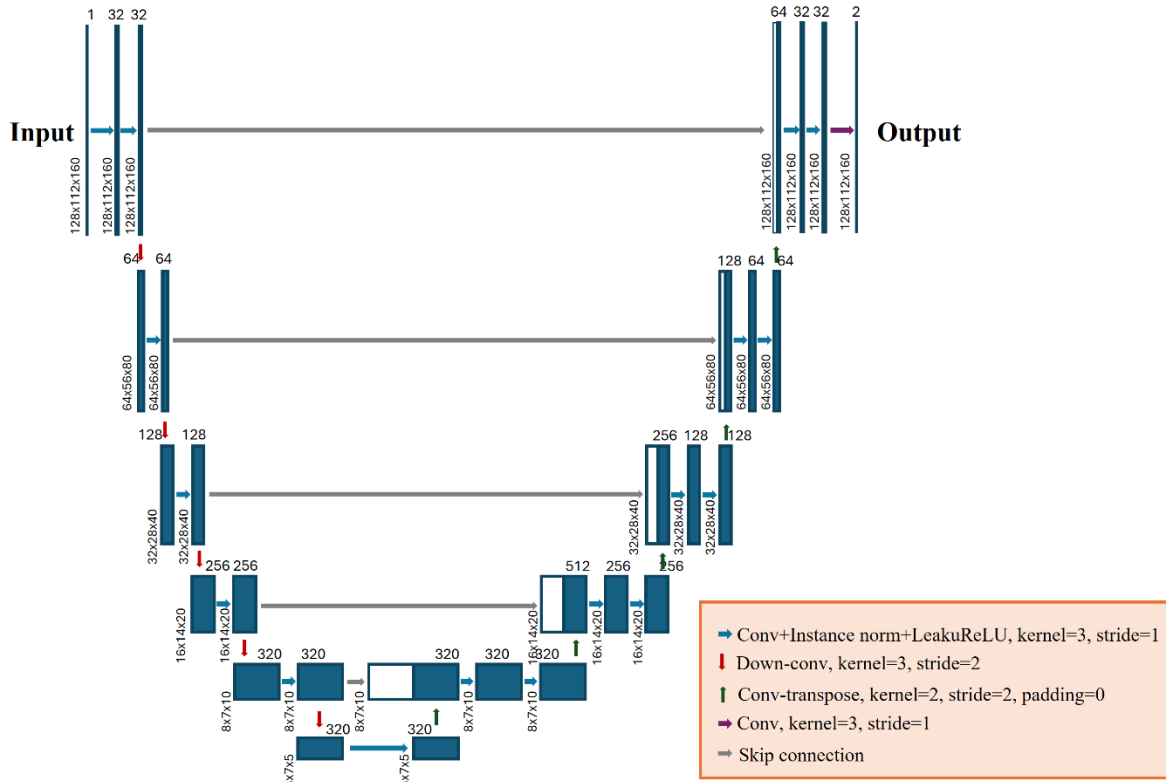


Figure4 Specific network structure (S2-1) in the VLSOM module

### 3. Results

After completing the training process, the proposed model was evaluated on a test set consisting of 57 cases using quantitative metrics including Centerline Dice (Cl-DICE<sup>[16]</sup>), Centerline Recall (Cl-Recall<sup>[17]</sup>), Recall and DICE. As mentioned in the introduction, the DICE value can only reflect global information, but cannot focus on the integrity and connectivity of the vessel structure. Therefore, our work mainly focuses on centerline-related indicators, such as Cl-DICE and Cl-Recall. The Higher Cl-Recall and Cl-Dice mean that more pulmonary vessel branches are correctly separated by the model, indicating a more complete and rich vascular tree segmentation result. Compared with nnUNet-v2 baseline, our model demonstrates superior performance in pulmonary vessel segmentation for both CTPA and NCCT data. The results are shown in **Table 1**.



**Table1 Pulmonary vessel segmentation results of CTPA and NCCT data**

CTPA		Artery	Vein	Artery	Vein	Artery	Vein	Artery	Vein
		CI-DICE	CI-DICE	CI-Recall	CI-Recall	Recall	Recall	DICE	DICE
nnUNet-v2		0.842	0.868	0.774	0.811	0.838	0.883	<b>0.870</b>	<b>0.896</b>
Our Method		<b>0.872</b>	<b>0.887</b>	<b>0.866</b>	<b>0.932</b>	<b>0.909</b>	<b>0.959</b>	0.864	0.843
NCCT		Artery	Vein	Artery	Vein	Artery	Vein	Artery	Vein
		CI-DICE	CI-DICE	CI-Recall	CI-Recall	Recall	Recall	DICE	DICE
nnUNet-v2		0.899	0.910	0.845	0.860	0.891	0.880	0.905	<b>0.884</b>
Our Method		<b>0.927</b>	<b>0.929</b>	<b>0.920</b>	<b>0.951</b>	<b>0.942</b>	<b>0.967</b>	<b>0.907</b>	0.869

As shown in the table, the method proposed in this paper has achieved a relatively significant improvement over the nnUNet-v2 in terms of the CI-Recall, CI-Dice and Recall metrics. This indicates that the model in this paper can segment more complete and intricate vascular tree branches. However, when using this method, it may lead to coarser segmentation results, which in turn caused a certain decrease in the DICE metric. Nevertheless, during clinical evaluations, this slight thickening of the vessels did not significantly affect the identification and analysis of the lumen structure. From both the global and local levels, we documented the actual segmentation results of the proposed model on the test data. It can be observed that our method can obtain more complete vascular branches. The overall comparison of the segmentation results is shown in **Figure5** and **Figure6**, and the comparison of local vascular structures is shown in **Figure7** and **Figure8**.

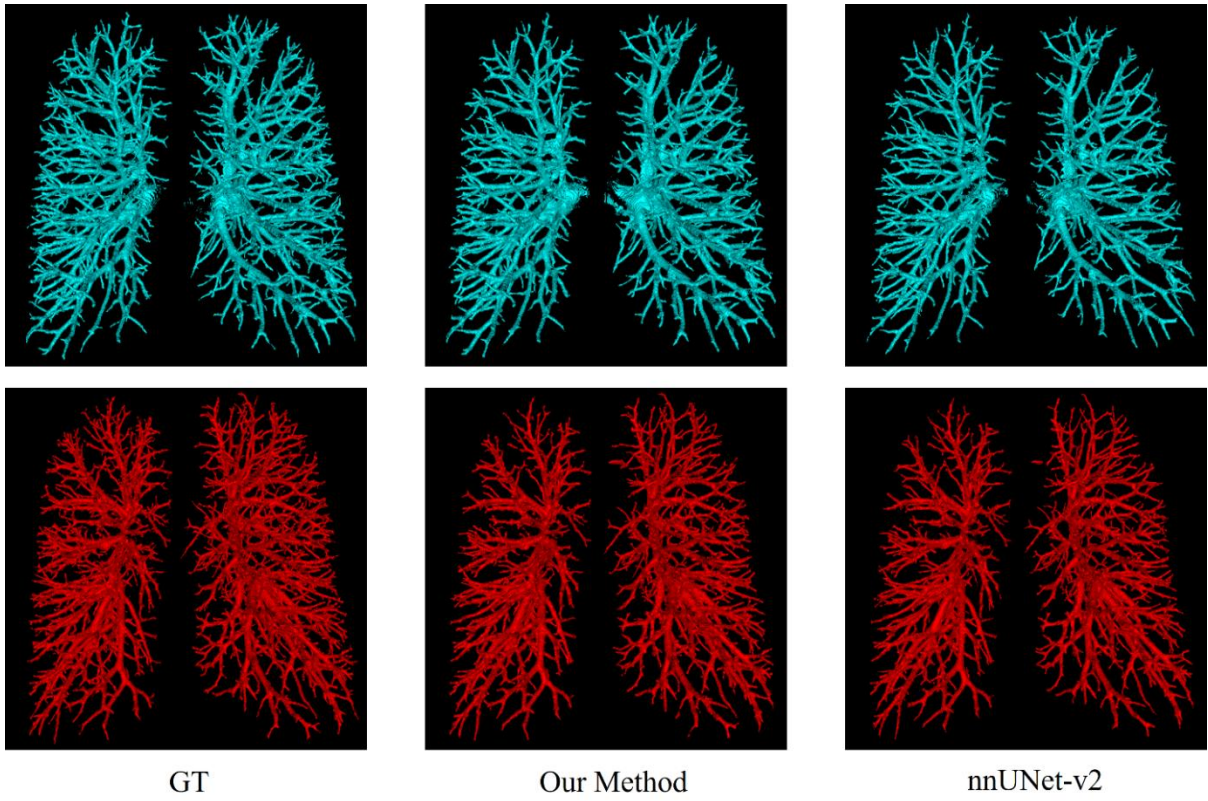


**Figure5** Example of global segmentation results of CTPA data

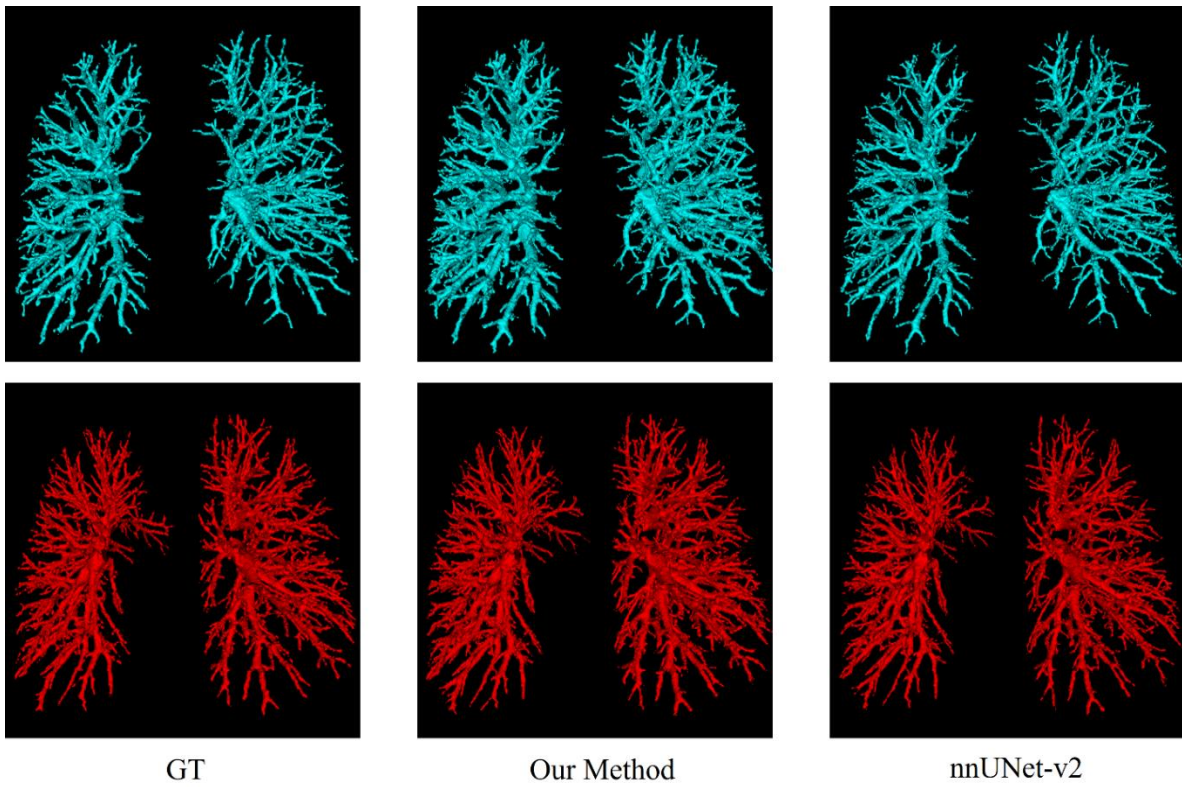


**Figure6** Example of global segmentation results of NCCT data

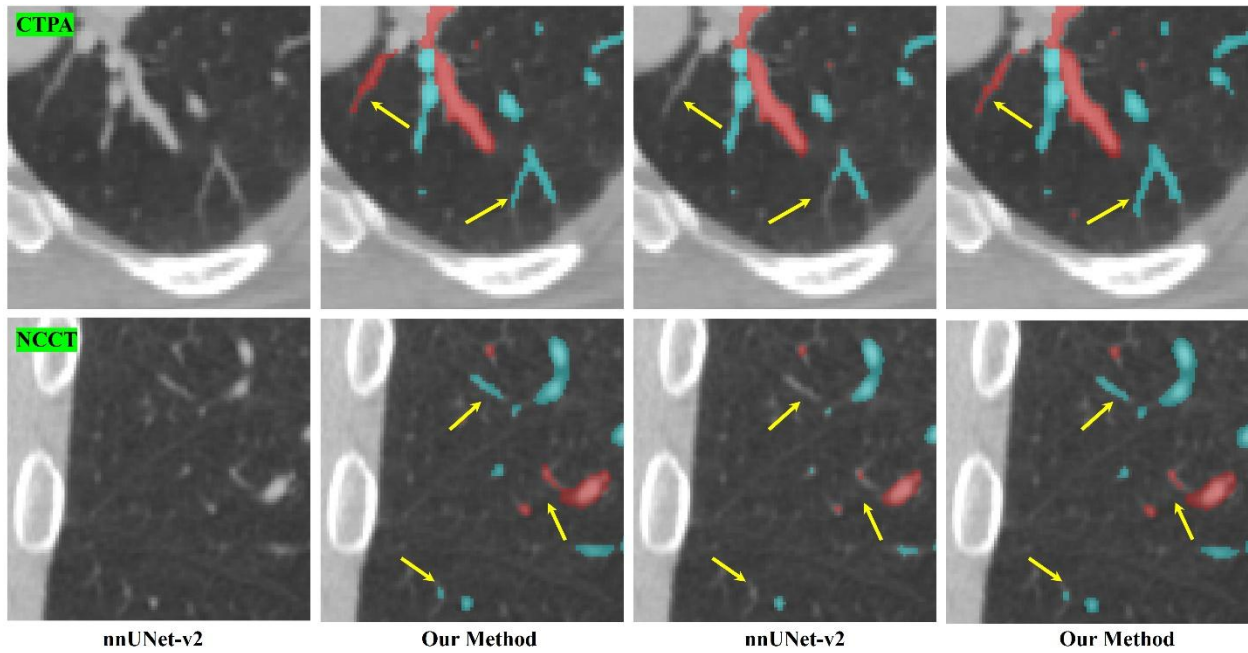


**Figure7** Example of local segmentation results for pulmonary vessels(2D)

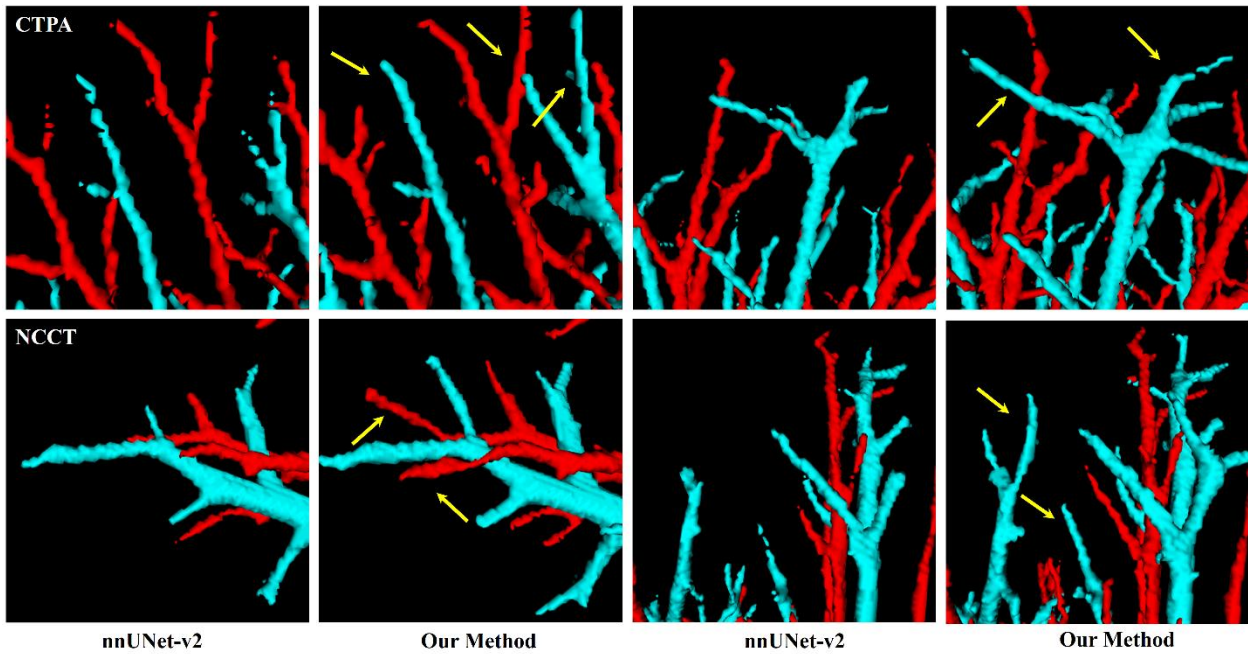


**Figure8** Example of local segmentation results for pulmonary vessels(3D)

## 4. Conclusion

This study introduced a 3D segmentation network with a Vessel Lumen Structure Optimization Module (VLSOM) to enhance pulmonary vessel segmentation performance. By leveraging combined learning from CTPA and NCCT data, the proposed method achieved automatic vascular segmentation both on contrast and non-contrast CT images, offering potential for clinical pulmonary vessel analysis and disease diagnosis. However, the current algorithm still has limitations in terms of clinical applicability. The primary challenges include insufficient segmentation accuracy for small vessels (the diameter is less than 1mm) and partial errors in artery-vein classification, particularly in complex or low-contrast regions. These issues may arise due to the difficulty of capturing fine details in medical images and the complexity of pulmonary vasculature.

Future improvements could focus on incorporating advanced techniques such as multi-scale feature extraction or attention mechanisms to better detect small vessels. Additionally, expanding the training dataset and integrating anatomical priors could help reduce classification errors and improve robustness. Despite these limitations, the proposed method represents a significant step forward in pulmonary vessel segmentation and demonstrates promising potential for clinical applications. Further refinement is needed to enhance its practical utility in real-world scenarios.

## Reference

- [1] Ye Y, Sing C W, Hubbard R, et al. Prevalence, incidence, and survival analysis of interstitial lung diseases in Hong Kong: a 16-year population-based cohort study[J]. *The Lancet Regional Health–Western Pacific*, 2024, 42.
- [2] Nabel E G. Cardiovascular disease[J]. *New England Journal of Medicine*, 2003, 349(1): 60-72.
- [3] Tarride J E, Lim M, DesMeules M, et al. A review of the cost of cardiovascular disease[J]. *Canadian Journal of Cardiology*, 2009, 25(6): e195-e202.
- [4] Hulten E A, Carbonaro S, Petrillo S P, et al. Prognostic value of cardiac computed tomography angiography: a systematic review and meta-analysis[J]. *Journal of the American College of Cardiology*, 2011, 57(10): 1237-1247.



- [5] Koelemay M J W, Nederkoorn P J, Reitsma J B, et al. Systematic review of computed tomographic angiography for assessment of carotid artery disease[J]. *Stroke*, 2004, 35(10): 2306-2312.
- [6] Pu J, Gezer N S, Ren S, et al. Automated detection and segmentation of pulmonary embolisms on computed tomography pulmonary angiography (CTPA) using deep learning but without manual outlining[J]. *Medical Image Analysis*, 2023, 89: 102882.
- [7] Guo X, Zhang P, Guo Y, et al. A Novel Method for Pulmonary Artery Segmentation from CTPA Images[C]//2024 2nd International Conference on Algorithm, Image Processing and Machine Vision (AIPMV). IEEE, 2024: 162-170.
- [8] Nguyen T N, Abdalkader M, Nagel S, et al. Noncontrast computed tomography vs computed tomography perfusion or magnetic resonance imaging selection in late presentation of stroke with large-vessel occlusion[J]. *JAMA neurology*, 2022, 79(1): 22-31.
- [9] Buzug T M. *Computed tomography*[M]//Springer handbook of medical technology. Berlin, Heidelberg: Springer Berlin Heidelberg, 2011: 311-342.
- [10] Chu Y, Luo G, Zhou L, et al. Deep learning-driven pulmonary artery and vein segmentation reveals demography-associated vasculature anatomical differences[J]. *Nature Communications*, 2025, 16(1): 2262.
- [11] Wang M, Qi S, Wu Y, et al. CE-NC-VesselSegNet: Supervised by contrast-enhanced CT images but utilized to segment pulmonary vessels from non-contrast-enhanced CT images[J]. *Biomedical Signal Processing and Control*, 2023, 82: 104565.
- [12] Armato III S G, McLennan G, Bidaut L, et al. The lung image database consortium (LIDC) and image database resource initiative (IDRI): a completed reference database of lung nodules on CT scans[J]. *Medical physics*, 2011, 38(2): 915-931.
- [13] Tang, Michael Chi Seng, and Soo Siang Teoh. "Blood vessel segmentation in fundus images using hessian matrix for diabetic retinopathy detection." 2020 11th IEEE Annual Information Technology, Electronics and Mobile Communication Conference (IEMCON). IEEE, 2020.
- [14] Isensee F, Jaeger P F, Kohl S A A, et al. nnU-Net: a self-configuring method for deep learning-based biomedical image segmentation[J]. *Nature methods*, 2021, 18(2): 203-211.

- [15] Milletari F, Navab N, Ahmadi S A. V-net: Fully convolutional neural networks for volumetric medical image segmentation[C]//2016 fourth international conference on 3D vision (3DV). Ieee, 2016: 565-571.
- [16] Shi P, Hu J, Yang Y, et al. Centerline boundary dice loss for vascular segmentation[C]//International Conference on Medical Image Computing and Computer-Assisted Intervention. Cham: Springer Nature Switzerland, 2024: 46-56.
- [17] Kirchhoff Y, Rokuss M R, Roy S, et al. Skeleton recall loss for connectivity conserving and resource efficient segmentation of thin tubular structures[C]//European Conference on Computer Vision. Cham: Springer Nature Switzerland, 2024: 218-234.